electronics

MDPI

Article

Reducing Noise and Impact of High-Frequency Torque Ripple Caused by Injection Voltages by Using Self-Regulating Random Model Algorithm for SynRMs Sensorless Speed Control

Yibo Guo, Lingyun Pan, Yang Yang *, Yimin Gong and Xiaolei Che

College of Physics, Jilin University, Changchun 130000, China; guoyb22@mails.jlu.edu.cn (Y.G.); ply@jlu.edu.cn (L.P.); gongym@jlu.edu.cn (Y.G.); chexl@jlu.edu.cn (X.C.)
* Correspondence: jlu_yang@jlu.edu.cn

Abstract: For the sensorless control in a low-speed range of synchronous reluctance motors (SynRMs), injecting random high-frequency (HF) square-wave-type voltages has become a widely used and technologically mature method. It can solve the noise problem of traditional injection signal methods. However, all injection signal methods will cause problems such as torque ripple, which causes speed fluctuations. This article proposes a self-regulating random model algorithm for the random injection signal method, which includes a quantity adaptive module for adding additional random processes, an evaluation module for evaluating torque deviation degree, and an updated model module that is used to receive signals from the other two modules and complete model changes and output random model elements. The main function of this algorithm is to create a model that updates to suppress the evaluation value deviation based on the evaluation situation and outputs an optimal sequence of random numbers, thereby limiting speed bias always in a small range; this can reduce unnecessary changes in the output value of the speed regulator. The feasibility and effectiveness of the proposed algorithm and control method have been demonstrated in experiments based on a 5-kW synchronous reluctance motor.

Keywords: HF voltage injection; SynRM; sensorless control; random number

check for updates

Citation: Guo, Y.; Pan, L.; Yang, Y.; Gong, Y.; Che, X. Reducing Noise and Impact of High-Frequency Torque Ripple Caused by Injection Voltages by Using Self-Regulating Random Model Algorithm for SynRMs Sensorless Speed Control. *Electronics* **2024**, *13*, 3327. https://doi.org/10.3390/electronics13163327

Academic Editor: Carlo Petrarca

Received: 16 July 2024
Revised: 7 August 2024
Accepted: 16 August 2024
Published: 22 August 2024

Copyright: © 2024 by the authors. Licensee MDPI, Basel, Switzerland. This article is an open access article distributed under the terms and conditions of the Creative Commons Attribution (CC BY) license (https://creativecommons.org/licenses/by/4.0/).

1. Introduction

Synchronous reluctance motors (SynRMs) exhibit advantages such as simple structure, ruggedness, high efficiency, wide speed range, and low cost. The price of rare earth metals for making permanent magnets is becoming increasingly high. In the future, SynRMs will receive a wider range of applications. In order to fully utilize these advantages, it is necessary to achieve sensorless speed control. The main methods to achieve sensorless control include using high-frequency signal injection, extended back electromotive force (EMF) or flux observers, Kalman Filter, etc. These methods can estimate the rotor position and speed, achieving sensorless control of the motor.

In [1–5], back EMF or flux observers are used; these methods have good performance in high-speed ranges. For SynRMs, because there is no permanent magnet on the rotor, the back EMF and flux linkages are very small at low-speed or zero-speed ranges, which means that these methods require additional operations [6] or need to be used in scenarios with extremely high sampling accuracy, which is impossible to adapt to all application conditions. And for the methods of using the Kalman filter [7,8], the calculations are enormous. So, these methods are difficult to achieve in most cases. Based on the above reasons, when SynRMs run in the low-speed range, the method of using high-frequency (HF) injection signals is usually chosen. This method has been widely used in speed sensorless control of various types of motors, with some injecting current signals [9–11] and others injecting voltage signals [12–20].

For general speed-control methods, the injection port can be set at the output end of the current regulator of the methods, which use voltage signals; this means that the injection voltage value will be more accurate. This is the reason that voltage signals are used more frequently than current signals. In [12], a square-wave-type voltage injection incorporated into the associated signal processing method is proposed which has been widely accepted. But, there is a very serious problem with the control method of injecting a fixed voltage signal, which is the noise problem. In order to solve this problem, it is no longer appropriate to inject fixed signals, and many methods of injecting random voltages have been proposed [13–16]. The method of pseudo-random voltage injection is more commonly used because it does not require changing the carrier frequency of pulse width modulation (PWM), making the control period more stable and the regulator coefficients easier to design. This article will improve the sensorless speed-control method based on the pseudo-random voltage injection method and prove that this method also has the function of reducing noise.

Another issue with the injection voltage method is that it introduces current harmonics, which cause additional torque ripple [21], further causing fluctuations in speed, thereby affecting sensorless speed control. This is because, unlike permanent magnet synchronous motors (PMSMs), the electromagnetic torque of SynRMs is the only reluctance torque. Therefore, the $i_d = 0$ control strategy commonly used in PMSMs is no longer applicable. During this operation, there is current on the d-q axis of the motor, and any direction of current fluctuation may cause torque fluctuation. The ripple can be suppressed by optimizing motor design [22] but cannot be minimized completely. There are also methods to reduce torque ripple by compensating for current [21,23] or injecting voltages in a special way [18]. But, from the analysis process of these methods, it can be seen that they heavily rely on the accuracy of position estimation and the stability of motor parameters. However, based on the saturation phenomenon of the SynRMs, those sensorless control methods of SynRMs as [16–18] often require the use of methods such as those proposed in [24] or [25] to calibrate the motor model in advance and the use of look-up-table methods during control to ensure the control successfully. In fact, the traditional HF voltage injection method is a saliency detection method for running in a low-speed range; the saturation phenomenon does not seriously affect the successful operation of sensorless control [19,20]. Therefore, it is not necessary to identify the motor parameters when the motor operates in the low-speed zone, which can ensure the universality and simple structure of the control method used.

In summary, in order to make the sensorless speed control of SynRMs effective, simple, and with low noise, it is necessary to use random voltage injection and minimize the impact of torque ripple on speed. At present, there is no suitable method to simultaneously consider the speed fluctuation caused by torque ripple under the premise of using random injection voltage. This article will analyze in detail the impact of torque ripple on speed when using random voltage injection for sensorless speed control of SynRMs. The impact of torque ripple on speed can be quantified and controlled within a very small range by using the proposed self-regulating random model algorithm. This algorithm can minimize speed fluctuations under the premise of using random voltage injection in a low-speed range.

The main contribution of this article is to propose the self-regulating random model algorithm. This algorithm has only three parts, which are one quantity adaptive module, one evaluation module, and one updated model module. This algorithm has a simple structure, low computational complexity, and can run independently without changing the structure of the original random voltages injection control framework. It is worth mentioning that this algorithm can be applied in a wide range of scenarios. In this article, the speed deviation degree caused by torque ripple is considered as the evaluation object. When applied to other scenarios, it is only necessary to change the evaluation object and evaluation method; the algorithm can update the active elements in the model and select the optimal random output sequence.

The rest of this article is organized as follows. The basic introduction of the sensorless control, which uses random square-wave-type voltage, is illustrated in Section 2. The

analysis of how injecting voltage can cause torque ripples and further cause speed bias, and the calculated effect of voltage used in the experiment on speed are presented in Section 3. In Section 4, the self-regulating random model algorithm is introduced in detail, and the operation mode and principle of each module are explained; the overall control diagram is shown. The power spectral density (PSD) calculation used to explain how this method can reduce noise is presented in Section 5. The effectiveness of algorithms, sensorless control methods, and the results of comparison of experimental effects on reducing speed fluctuation are shown in Section 6. Finally, Section 7 concludes this article.

2. Random Square-Wave-Type Voltage Injection Sensorless Control Strategy for SynRMs

2.1. The Mathematical Model of a SynRM

The model of a SynRM in a dq-axis synchronous frame under the steady state can be expressed as

$$\begin{cases} u_d = R_s i_d + L_d \frac{di_d}{dt} - \omega_{re} L_q i_q \\ u_q = R_s i_q + L_q \frac{di_q}{dt} + \omega_{re} L_d i_d \end{cases} \tag{1}$$

where u_d, u_q, R_s, i_d, i_q, ω_{re}, L_d, L_q are d-axis stator voltage, q-axis stator voltage, stator resistance, d-axis stator current, q-axis stator current, motor electrical speed, d-axis inductance, and q-axis inductance, respectively.

The electromagnetic torque mathematic model and the motor motion equation can be expressed as

$$T_e = \frac{3P}{2}\left(L_d - L_q\right) i_d i_q \tag{2}$$

$$\mathrm{J}\frac{d\omega_r}{dt} = T_e - T_L - B\omega_r \tag{3}$$

where P is the number of pole pairs; J is the rotor inertia; T_L is the load torque; ω_r is motor speed, which is calculated as $\omega_r = \omega_{re}/P$, and B is the damping coefficient.

2.2. Sensorless Control Based on Square-Wave-Type Voltage Injection

It has been proposed in [12] that when the injection voltage is described as

$$U_{d,inj} = \begin{cases} U_h & half\ duty \\ -U_h & otherwise \end{cases} \quad (U_h > 0), U_{q,inj} = 0 \tag{4}$$

as shown in Figure 1, the high frequency of the corresponding induced current in the $\alpha\beta$-axis can be described as

$$\begin{cases} \Delta i_{\alpha,h,k} = \frac{U_{d,inj,k-1}\Delta T}{L_d} \times \cos\theta_{re} \\ \Delta i_{\beta,h,k} = \frac{U_{d,inj,k-1}\Delta T}{L_d} \times \sin\theta_{re} \end{cases} \tag{5}$$

where the subscript k represents the k-th data; ΔT is the interval time between two adjacent data sampling; θ_{re} is the electrical angle of the rotor position; $\Delta i_{\alpha,h,k}$ and $\Delta i_{\beta,h,k}$ are high-frequency parts of the $\alpha\beta$-axis current variation, which can be obtained by

$$\begin{cases} \Delta i_{\alpha,h,k} = i_{\alpha,h,k} - i_{\alpha,h,k-1} \\ \Delta i_{\beta,h,k} = i_{\beta,h,k} - i_{\beta,h,k-1} \end{cases} \tag{6}$$

According to (5), if a matrix is established as

$$e_n = \begin{bmatrix} \Delta i_{\alpha,h} \\ \Delta i_{\beta,h} \end{bmatrix} \tag{7}$$

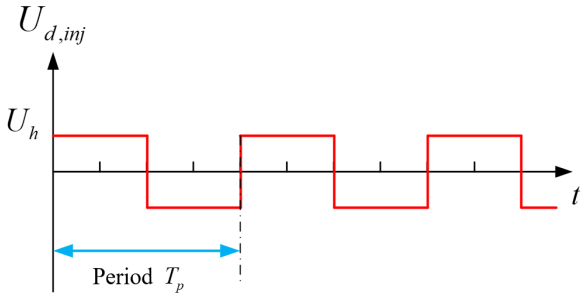

Figure 1. The schematic diagram of the injection voltage of the *d*-axis.

It is easy to obtain that

$$\frac{de_n}{dt} = \omega_{re} R e_n, \text{ where } R = \begin{bmatrix} 0 & -1 \\ 1 & 0 \end{bmatrix} \tag{8}$$

The motor's electrical speed ω_{re} can be estimated by an adaptive speed estimator, which is used in [3].

$$\frac{d\tilde{e}_n}{dt} = \omega_{re} R \tilde{e}_n + \begin{bmatrix} g & 0 \\ 0 & g \end{bmatrix} (\tilde{e}_n - e_n) \tag{9}$$

where the values with symbol ~ mean estimated values; g is the feedback gain of the adaptive estimator. For the convenience of designing the coefficients in the adaptive speed estimator, the matrix e_n can be normalized. Another advantage of normalization is that there is no need to consider changes in L_d, and there is no parameter sensitivity issue in the entire control process. The configuration of the adaptive speed estimator is shown in Figure 2; by obtaining the high-frequency current component of the α-β axis and combining it with formulae (6)–(9), the motor speed can be obtained. Further, the electrical angle of the rotor can be calculated by a phase-locked loop (PLL), which is shown in Figure 3. Unlike directly integrating the motor speed to obtain the angle, this method can quickly compensate for the error between the true angle and the estimated angle. Based on this advantage, this method can avoid estimating the initial angle of the motor, and even if there is an error in estimating the speed, it can ensure that all coordinate transformations can be successfully achieved. The sensorless control block diagram composed of an adaptive speed estimator and PLL is shown in Figure 4. This is the original voltage injection method (OVIM). The sensorless control method proposed in [16] is also applicable, but the method proposed in this article uses an adaptive speed estimator, which ensures that the estimated speed has smaller fluctuations. Due to further analysis of velocity fluctuations in the following text, it is not suitable to use angle error integration to obtain motor velocity.

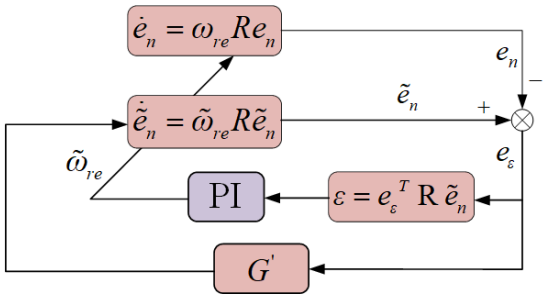

Figure 2. Configuration of adaptive speed estimator.

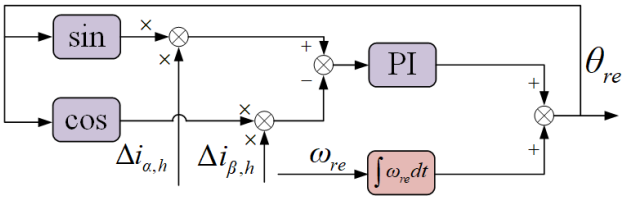

Figure 3. PLL for calculating electrical angle.

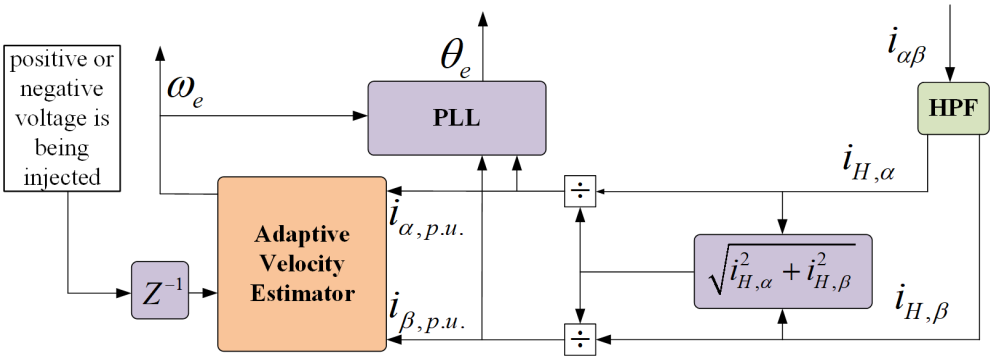

Figure 4. Using adaptive velocity estimator and PLL to obtain motor speed and electrical angle.

2.3. Random High-Frequency Square-Wave-Type Voltage Injection Method Description

The high-frequency SynRM model of the square-wave-type voltage injection method is expressed as

$$\begin{bmatrix} U_{d,inj} \\ U_{q,inj} \end{bmatrix} = \begin{bmatrix} L_d & 0 \\ 0 & L_q \end{bmatrix} \frac{d}{dt} \begin{bmatrix} i_{d,h} \\ i_{q,h} \end{bmatrix} \tag{10}$$

where $i_{d,h}$ and $i_{q,h}$ are high-frequency part of the current in dq-axis.

It is obvious that if the injection voltages in the d-axis are of the square-wave-type, the corresponding induced currents in the d-axis are of the triangular-wave-type. A square-wave form function $u_f(t, T_p, \varphi)$ and a triangular-wave form function $i_f(t, T_p, \varphi)$ can be defined as

$$\begin{gathered} u_f(t, T_p, \varphi) = \begin{cases} 1, 0 \le t_{mod}\left(t - \frac{\varphi}{360^\circ}, T_p\right) \le \frac{T_p}{2} \\ -1, \frac{T_p}{2} < t_{mod}\left(t - \frac{\varphi}{360^\circ}, T_p\right) < T_p \end{cases} \\ \left(\begin{array}{l} if\ t_{mod}(t, T_p) < 0, t_{mod}(t, T_p) = t_{mod}(t, T_p) + T_p \\ if\ t_{mod}(t, T_p) > T_p, t_{mod}(t, T_p) = t_{mod}(t, T_p) - T_p \end{array} \right) \end{gathered} \tag{11}$$

$$i_f(t, T_P, \varphi) = \frac{1}{T_P} \int_0^t u_f(t, T_P, \varphi) dt \tag{12}$$

where T_p is the period of the injecting voltage; φ denotes the phase of the voltage, and in this article, it only has the right values, $\varphi = \{0^\circ, 45^\circ, 90^\circ, 135^\circ, 180^\circ, 225^\circ, 270^\circ, 315^\circ\}$ and $t_{mod}(t, T) = t \bmod T$. The voltage and induced current at these eight phases are shown correspondingly in Figure 5.

T_s is the period of the PWM wave and is also the period of the control, considering that for eliminating the effect of non-ideal characteristics of the inverter and the third harmonics in the position estimation error [26] and to ensure fast response of the adaptive speed estimator, the periods T_p of the injection voltages in this article are set as $8T_s$ and $4T_s$. Twelve voltages have been set up. In order to facilitate the calculation of torque deviation degree. The corresponding numbers for the amplitude, period, and phase of these twelve voltages are shown in Table 1. Randomly injecting these twelve voltages, combined with the aforementioned sensorless control strategy, can achieve sensorless control of SynRMs. This method is called the random voltage injection method (RVIM).

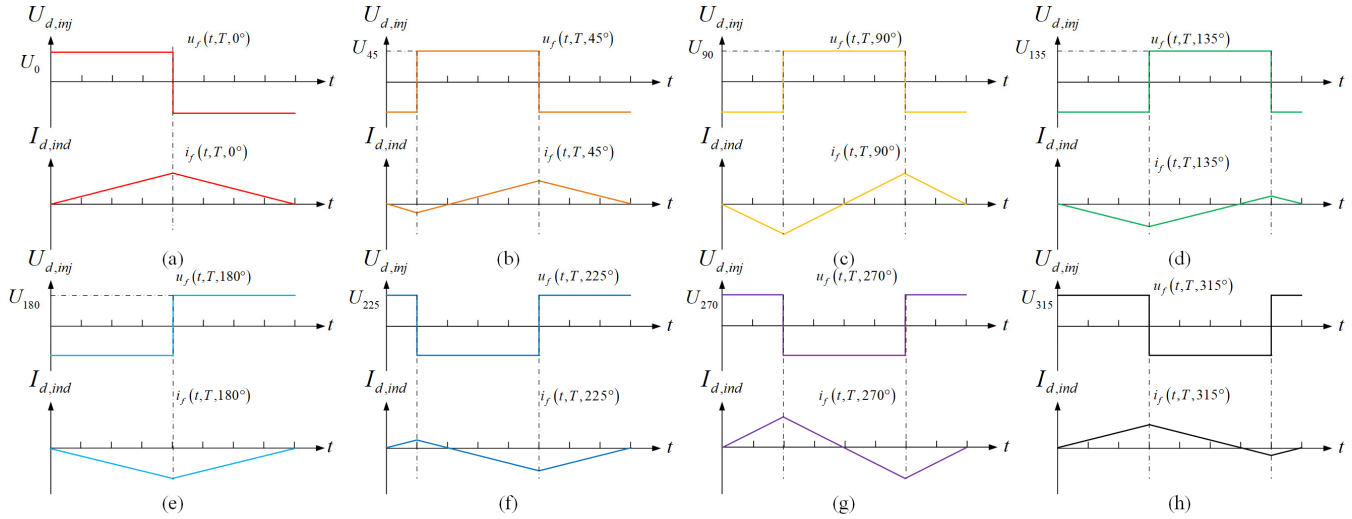

Figure 5. The schematic diagram of the eight basic injection voltages and corresponding induced currents in *d*-axis. (**a**) $\varphi = 0°$. (**b**) $\varphi = 45°$. (**c**) $\varphi = 90°$. (**d**) $\varphi = 135°$. (**e**) $\varphi = 180°$. (**f**) $\varphi = 225°$. (**g**) $\varphi = 270°$. (**h**) $\varphi = 315°$.

Table 1. Information of Twelve Voltages.

Number	1	2	3	4	5	6	7	8	9	10	11	12
Amplitude (V)	15		30		15		30	15	30	60	30	60
Period (s)	$8T_s$								$4T_s$			
Phase	0°	45°	90°	135°	180°	225°	270°	315°	0°	90°	180°	270°

3. Torque Ripple Analysis

3.1. The Torque Ripple Phenomenon Caused by Injected Voltage

The voltage injection sensorless control method is a method of determining the electrical angle and electrical speed of the rotor by analyzing the characteristics of the induced current and obtaining the saliency detection of the rotor. Induced current is inevitable, but it can cause high-frequency torque ripple, which affects the speed control of the motor. For the sensorless speed control of SynRMs, it is necessary to analyze torque ripple and minimize its impact on speed.

The torque ripple phenomenon caused by injected voltage has been analyzed in [19,22]. Due to the fact that the frequency of injected voltage is extremely high relative to the speed-control frequency, according to Equation (2), torque bias within an injection cycle can be expressed as

$$\Delta T_e = \frac{3P}{2}\left(L_d - L_q\right) i_q \Delta i_d \tag{13}$$

Neglecting changes in friction torque and load torque, the impact of this torque bias on motor speed can be calculated using Equation (3)

$$\Delta \omega_r = \frac{1}{J}\Delta T_e \Delta t = K(\Delta i_d \Delta t) \tag{14}$$

$$K = \frac{3P}{2J}\left(L_d - L_q\right) i_q \tag{15}$$

Within an injection cycle, the changes in current and inductance can be ignored, so K can be considered a constant. It can be seen that the speed change value is directly proportional to the product of the *d*-axis current change value and unit time, which means that the impact of torque ripple caused by the injected voltage on speed is proportional

to the area enclosed by the induced current and the time axis. Taking injection voltages numbered 1 and 2 in Table 1 as examples to calculate their impact on speed, the reference figure is shown in Figure 6. S_1 and S_2 are the areas enclosed by the induced current and time axis for these two injection voltages.

$$S_1 = \frac{1}{2} \cdot 8T_s \cdot K \frac{U_1}{L_d} \cdot 4T_s = 16KT_s^2 \frac{U_1}{L_d} \tag{16}$$

$$S_2 = -\frac{1}{2} \cdot 2T_s \cdot K \frac{U_2}{L_d} \cdot T_s + \frac{1}{2} \cdot 6T_s \cdot K \frac{U_2}{L_d} \cdot 3T_s = 8KT_s^2 \frac{U_2}{L_d} \tag{17}$$

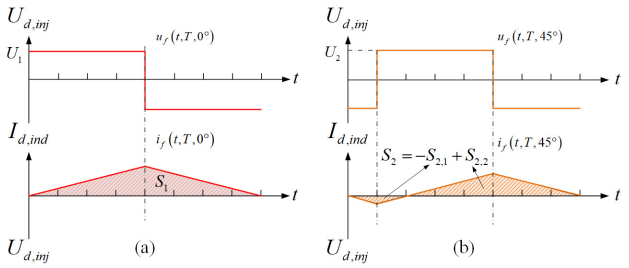

Figure 6. Reference diagram for calculating the impact of injected voltage on speed. (**a**) No.1. (**b**) No.2.

For coefficients shown in Table 1, $U_1 = U_2$; therefore, $S_1 = 2S_2$. If the speed bias value caused by the injection voltage numbered 2 is the unit of 1, the remaining bias values should be calculated, as shown in Table 2.

Table 2. Speed bias caused by twelve voltages.

Speed Bias	−2	−1	0	1	2
Number	5	4, 6, 11	3, 7, 10, 12	2, 8, 9	1

In order to ensure sensorless speed control and minimize the impact of injected voltage, it is necessary to ensure that the total speed bias is around 0. This can ensure a stable output of the speed loop regulator and prevent overall speed fluctuations and oscillations.

3.2. Analysis of the Torque Ripple Phenomenon in SynRMs

According to (15)–(17), the magnitude of the speed bias caused by injected voltage is related to the inductance values of L_d and L_q, and q-axis current i_q. And when the operating state of the motor changes, such as acceleration, deceleration, and changing the load, the current value changes. Due to the saturation effect of SynRMs, as shown in Figure 7, its dq-axial inductance value will change with the variation in axial current. This means that the relative ratio of the influence of each voltage on speed remains unchanged, but the absolute value always changes.

The above characteristics impose stricter restrictions on control. In order to ensure that the speed does not fluctuate even when the motor's operating state changes, it is necessary to maintain the speed bias around 0 at all times. This is difficult for RVIM to achieve. This control method only needs to randomly generate one random number and then select the corresponding voltage for injection. However, random numbers generated by most programming languages exhibit oscillations and periodicity over a long period of time. If there is also oscillation in the torque deviation caused by the corresponding injection voltage, it may cause speed fluctuations. Figure 8 shows the speed bias calculated based on Table 2 when operating the motor using RVIM. From Figure 8, it can be seen that the injection voltage has a significant impact on the speed.

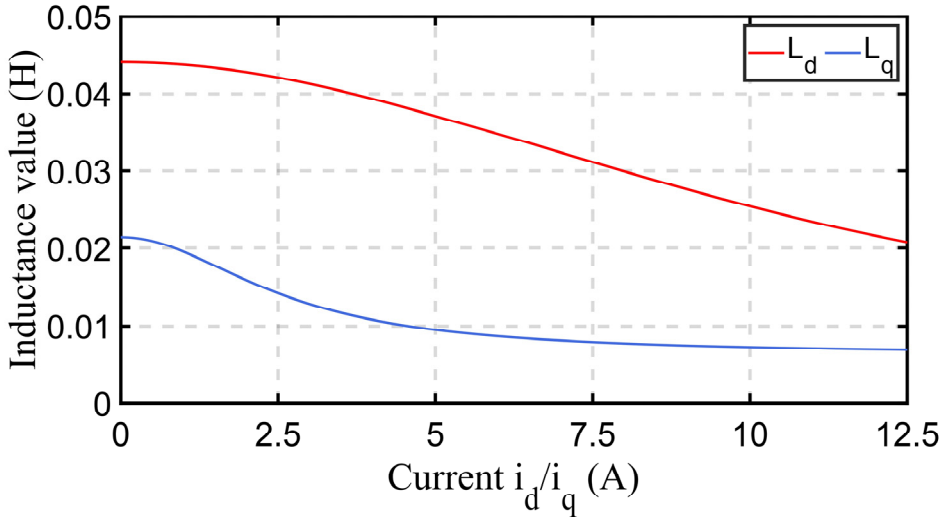

Figure 7. The variation in SynRM *dq*-axis inductance due to saturation effect.

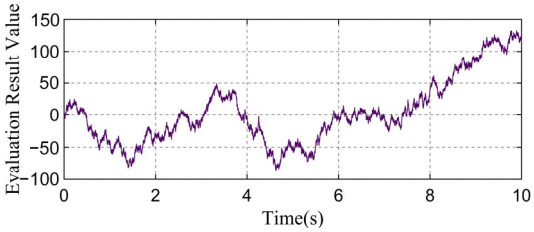

Figure 8. The summed-up value of the speed bias of using RVIM according to Table 2.

4. Introduction of the Proposed Self-Regulating Random Model Algorithm

In this section, the proposed self-regulating random model algorithm will be introduced in detail. The proposed self-regulated random model algorithm is created as a Simulink model and uploaded to Supplementary Materials. The use of a self-regulating random model algorithm with multiple random processes can eliminate the fluctuation impact of the generated random numbers and the injection voltage they represent on speed control. This algorithm can increase the randomness of injection voltage usage and ensure that the speed bias is around 0 in every short time duration.

4.1. Operation Mode of the Self-Regulating Random Model Algorithm

The overall diagram of the self-regulating random model algorithm is shown in Figure 9. The controller needs to generate three random numbers to help the algorithm process.

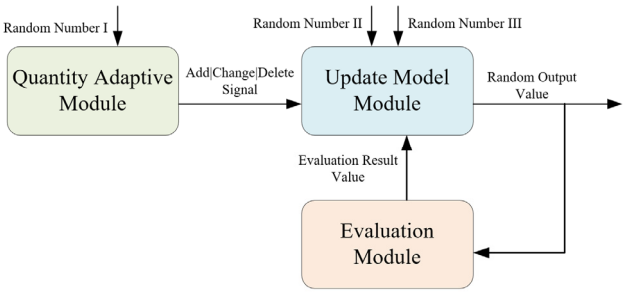

Figure 9. Overall diagram of self-regulating random model algorithm.

The main function of the algorithm is to create a model with 12 elements; some are in an activated state, while others are in an inactive state. This model continuously updates

the activated elements in the model based on the combination of evaluation result value and model-activated element quantity adjustment signals and finally outputs a random number from these activated elements to ensure that the evaluation result value is always maintained near the expected value. This can meet our requirement that the speed bias is always around 0.

At the initial condition, it is necessary to set the model with 3 to 7 activated elements; elements are the numbers from 1 to 12. Each number corresponds to its assigned voltage.

4.2. Operation Mode of the Quantity Adaptive Module

The principle diagram of the quantity adaptive module is shown in Figure 10, which is the law on how to update the model. This module is used to randomly generate signals of the way how to change the model. As can be seen from Figure 10, the module is divided into three regions; when the Random Number I, ranging from 0 to 1, belongs to three different regions, the module will output Add signal, Change signal, and Delete signal separately. The probability of generating various signals varies with the number of activated elements in the model. For example, if the number of activated elements in the model is five, there is a 50% probability that the module will generate a Delete signal, and when a probability is 25%, the module will generate an Add signal or a Change signal.

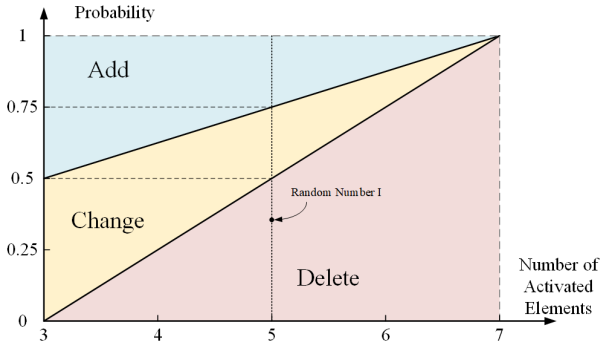

Figure 10. Principle diagram of the quantity adaptive module.

4.3. Operation Mode of the Evaluation Module

The theme structure of the evaluation module is a simple accumulator, which receives the random output value of the algorithms of the previous cycle, finds it in Table 2, records the speed bias generated by this output, accumulates the previous results, and outputs the new evaluation result value (V) to the Update Model Module. For other methods of suppressing torque fluctuations, complex mixed calculations of motor parameters are required, and control through the design of regulators is necessary. The computational complexity of the method proposed in this article only exists in this module, consisting of simple addition and subtraction of positive integers.

4.4. Operation Mode of the Update Model Module

The operation mode diagram of the Update Model Module is shown in Figure 11. Firstly, receive the signal from the quantity adaptive module and judge how to change the model. If an Add Signal is received, run Add Module; if a Delete Signal is received, run Delete Module; if a Change Signal is received, run both Add Module and Delete Module.

Every time the Add Module is run, it receives the state of the model, which is shown in Figure 11b; the red numbers mean elements that are activated, and the others are inactive. Add Module is used to select one of those inactive elements and change it to an activated state. Receive evaluation result value (V) from the evaluation module and make judgments. If $V > 0$, run Reduce Evaluation Value Module (REVM) with ①; if $V < 0$, run Increase Evaluation Value Module (IEVM) with ②; if $V = 0$, run Random Module (RM) with ③. The numbers ①, ②, ③ indicate the collections of inactive elements in the model. But ① removes 1, 2, 8, 9, which can increase the value of V; ② removes 4, 5, 6, 11.

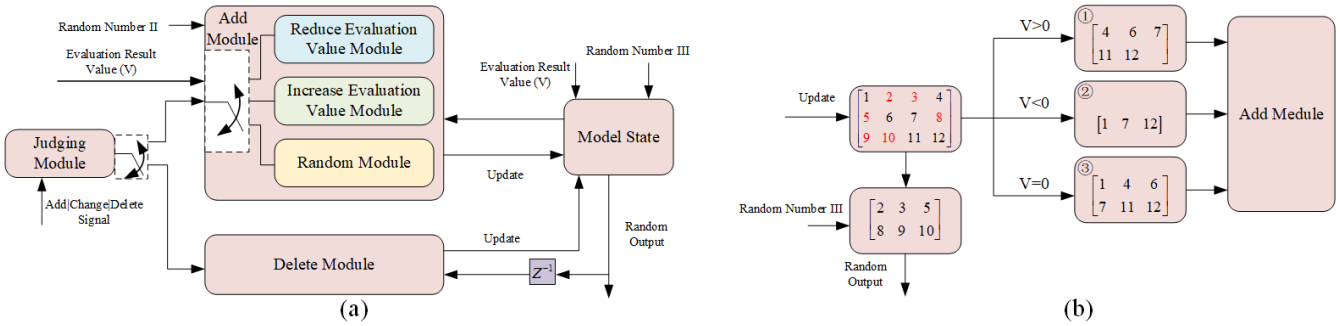

Figure 11. Update Model Module. (**a**) Overall logic diagram. (**b**) Schematic diagram of model state changes.

Every time the Delete Module is run, it receives random output from the algorithm of the previous cycle and changes this element to inactive to complete the update.

From a macro perspective, there are two trends in the changes in the elements within the model, adding elements that reduce the deviation of evaluation values and the repetition of the same element. The model is constantly changing toward the optimal model at the moment of using this algorithm, so combining random numbers to randomly output values for elements within the model can also be considered the optimal random output.

4.5. Sensorless Control Using Self-Regulating Random Model Algorithm

The overall flowchart of using the output of the self-regulating random model combined with Table 1 for pseudo-random voltage injection is shown in Figure 12. The output of this algorithm will be used to control which voltage is injected, and the whole sensorless speed-control system is shown in Figure 13. This method can be called a self-regulating random model method (SRRMM). Speed and current controls are implemented using Proportional–Integral (PI) regulators. A Low-Pass Filter (LPF) is used to filter out induced current to ensure signal stability. A High-Pass Filter (HPF) is used to extract induced current for sensorless control. The cutoff frequencies of LPF and HPF can both be set to $\frac{\pi}{32T_s}$.

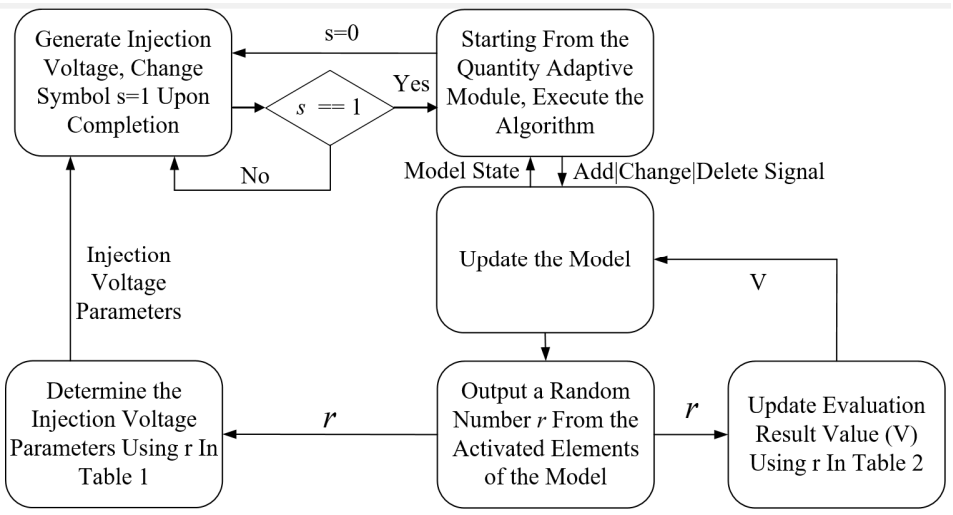

Figure 12. Flowchart of using the self-regulating random model algorithm to output injection voltage.

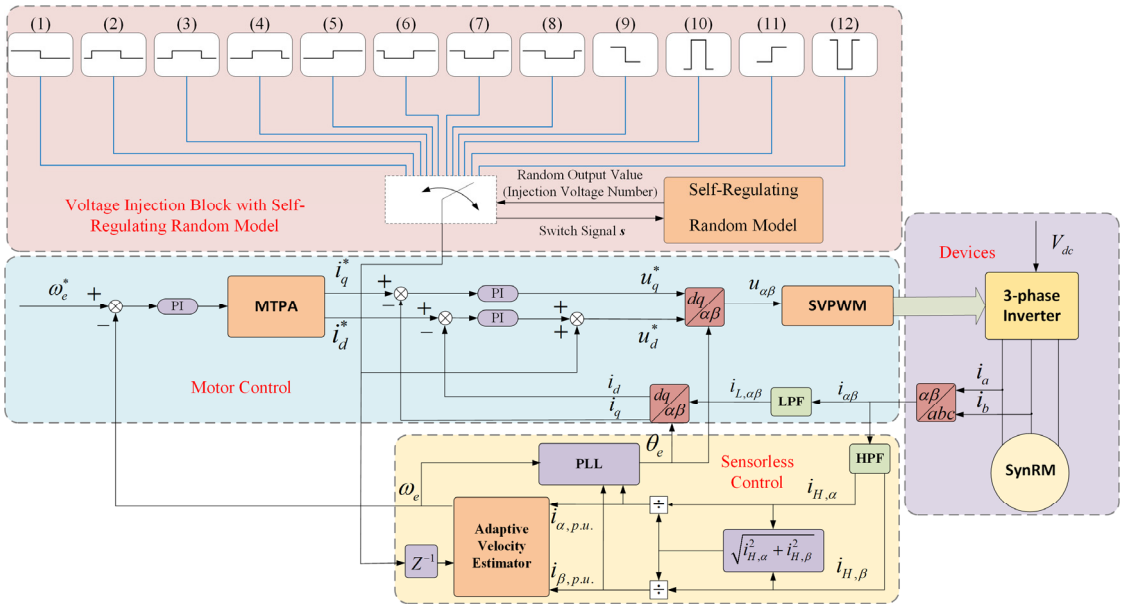

Figure 13. Block diagram of speed sensorless control system for SynRMs using self-regulating random model algorithm.

5. Analysis of PSD

Using a fixed frequency injection voltage can cause sharp noise, while the SRRMM proposed in this article uses pseudo-random injection voltage, which can achieve the function of reducing noise. Usually, the calculation of current PSD is used to demonstrate that PSD can effectively represent the distribution of energy in the frequency spectrum. The PSD values can be calculated using the following equation [27,28]:

$$S(f) = \frac{1}{E_T[T_p]} \left\{ \overbrace{E_{T,\varphi}\left[|I(f)|^2\right] - \left|E_{T,\varphi}[I(f)]\right|^2}^{continuous\ component} \quad \overbrace{\frac{1}{E_T[T_p]}\left|E_{T,\varphi}[I(f)]\right|^2 \sum_{k=-\infty}^{k=+\infty} \delta(f - kf_i)}^{discrete\ component} \right\} \tag{18}$$

where operator $E[]$ denotes mathematical expectation; $\delta()$ stands for the unit impulse function; $I(f)$ is the Fourier transform during one cycle.

For the twelve voltages, regardless of whether the period is $4T_s$ or $8T_s$, they all have a voltage with the phases of $\varphi = 0°, 90°, 180°, 270°$. The Fourier transform results of their induced current are as follows:

$$\begin{cases} I_{0°}(f, T_p) = \frac{1}{\pi^2 f^2 T_p}\left[2\left(1 - e^{-j2\pi f T_p}\right) + (2j\pi f T_p + 1)\left(e^{-j2\pi f T_p} - e^{-j\pi f T_p}\right)\right] \\ I_{90°}(f, T_p) = \frac{-1}{\pi^2 f^2 T_p}\left[2\left(e^{-j\frac{\pi}{2} f T_p} - e^{-j\frac{3\pi}{2} f T_p}\right) + \left(e^{-j2\pi f T_p} - 1\right)\right] \\ I_{180°}(f, T_p) = \frac{-1}{\pi^2 f^2 T_p}\left[2\left(1 - e^{-j2\pi f T_p}\right) + (2j\pi f T_p + 1)\left(e^{-j2\pi f T_p} - e^{-j\pi f T_p}\right)\right] \\ I_{270°}(f, T_p) = \frac{1}{\pi^2 f^2 T_p}\left[2\left(e^{-j\frac{\pi}{2} f T_p} - e^{-j\frac{3\pi}{2} f T_p}\right) + \left(e^{-j2\pi f T_p} - 1\right)\right] \end{cases} \tag{19}$$

where $T_p = \{4T_s, 8T_s\}$.

For the voltages with the period of $8T_s$, there are also four phases of φ = 45°, 135°, 225°, 315°. The amplitudes of the extreme values reached by the induced current are 0.5 and 0.25. The Fourier transform results of their induced current are as follows:

$$\begin{cases} I_{45^\circ}(f,T_p) = \frac{1}{2\pi^2 f^2 T_p}\left[1-e^{-j2\pi fT_p}+2\left(e^{-j\frac{5\pi}{4}fT_p}-e^{-j\frac{\pi}{4}fT_p}\right)\right] \\ I_{135^\circ}(f,T_p) = \frac{1}{2\pi^2 f^2 T_p}\left[1-e^{-j2\pi fT_p}+\left(2-j\frac{3\pi}{2}fT_p\right)\left(e^{-j\frac{7\pi}{4}fT_p}-e^{-j\frac{3\pi}{4}fT_p}\right)\right] \\ I_{225^\circ}(f,T_p) = \frac{-1}{2\pi^2 f^2 T_p}\left[1-e^{-j2\pi fT_p}+2\left(e^{-j\frac{5\pi}{4}fT_p}-e^{-j\frac{\pi}{4}fT_p}\right)\right] \\ I_{315^\circ}(f,T_p) = \frac{-1}{2\pi^2 f^2 T_p}\left[1-e^{-j2\pi fT_p}+\left(2-j\frac{3\pi}{2}fT_p\right)\left(e^{-j\frac{7\pi}{4}fT_p}-e^{-j\frac{3\pi}{4}fT_p}\right)\right] \end{cases} \tag{20}$$

where $T_p = 8T_s$.

It has been proved many times that if the injection signal frequencies only have odd times Least common multiple, the PSD will have discrete harmonics [14]. The period time of the voltages selected in this article are $4T_s$ and $8T_s$, respectively. So, for the system proposed in this article, there must be no discrete harmonics. Moreover, $I_{0^\circ}(f) = -I_{180^\circ}(f)$; $I_{90^\circ}(f) = -I_{270^\circ}(f)$; $I_{45^\circ}(f) = -I_{225^\circ}(f)$; $I_{135^\circ}(f) = -I_{315^\circ}(f)$. And from the operation mode of the algorithm, it can be seen that the probability of voltage injection with numbers 3, 7, 10, and 12 is the same, with a probability of about 10.530%, and the probability of the other eight voltages is about 7.235%. Equation (18) is finally reduced as

$$S(f) = \frac{1}{E_T[T_p]} E_{T,\varphi}\left[|I(f)|^2\right] \tag{21}$$

The specific result of the PSD of the induced current in the SRRMM can be expressed as

$$\begin{aligned} S(f) = {} & \tfrac{1}{4T_s}\left(0.1447|I_{0^\circ}(f,4T_s)|^2+0.2106|I_{90^\circ}(f,4T_s)|^2\right)+ \\ & \tfrac{1}{8T_s}(0.1447|I_{0^\circ}(f,8T_s)|^2+0.1447|I_{45^\circ}(f,8T_s)|^2+ \\ & 0.2106|I_{90^\circ}(f,8T_s)|^2+0.1447|I_{135^\circ}(f,8T_s)|^2) \end{aligned} \tag{22}$$

For OVIM which uses fixed frequency voltage, the result is

$$S(f) = \frac{1}{T_p}\left|I_{0^\circ}(f,T_p)\right|^2 \tag{23}$$

The control frequency used in this article is 10 kHz, which means T_s = 0.0001 s. The three PSD results of SRRMM and two OVIM with the period of $4T_s$ and $8T_s$, with voltage numbers 1 and 9 in Table 1, can be plotted. Usually, due to the small amplitude of PSD results, they take the logarithm based on ten and multiply it by ten. The processed results are shown in Figure 14. From the figure, it can be seen that the SRRMM smoothly disperses the induced current energy to various frequencies without any outliers appearing. This means that there will be no high-decibel noise of a certain frequency.

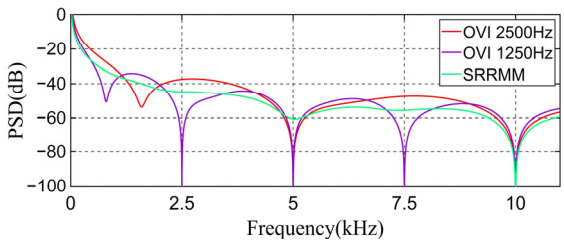

Figure 14. PSD results of the induced current of three different control methods.

6. Experimental Research

The experimental platform used is shown in Figure 15, where an eddy current dynamometer is used to apply load and verify the accuracy of the sensorless control of the motor speed estimation; the current probe is used to sample the phase current; a signal oscilloscope is used to record and display current signals, and the PC is used to communicate and control with the motor controller. The controller uses the chip RXR5F524T8ADFM. The parameters of the 5-kw motor are displayed in Table 3. The experimental verification is mainly divided into four steps. Firstly, it will be verified that the proposed self-regulating random model algorithm can be operated effectively. Secondly, various experiments are used to verify that this method can reduce the impact of torque ripple on sensorless speed control. Finally, it will be verified that the method used in this paper can effectively reduce noise.

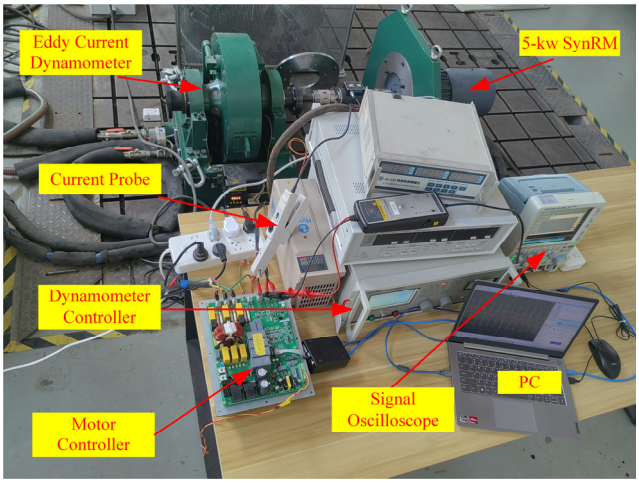

Figure 15. Experimental platform display diagram.

Table 3. Parameters of the 5-kW SynRM.

Parameter	Value
Pole Pairs	2
Resistance	0.25 Ω
Rated Current	12.5 A
Rated Voltage	380 V
D-Axis Inductance	43.9 mH
Q-Axis Inductance	22.1 mH

6.1. Validation of Self-Regulating Random Model Algorithm Performance

The specific operation mode of the self-regulating random model algorithm proposed in this article has been introduced in detail in Section 4. In order to prove the successful operation of this algorithm, running the motor using SRRMM for about 25 s, important parameters of each module of the algorithm are recorded based on the operating principles of the three modules included in the algorithm.

The main function of the quantity adaptive module is to output signals on how the model changes while also ensuring that the number of elements in the model has a certain degree of randomness. The results between 12 s and 12.1 s of the recorded output signal of the module and the number of elements in the model are shown in Figure 16. Regarding the Add | Change | Delete signal shown in Figure 16, if it is 1, it means the output is an Add signal; if it is 2, it means the output is a Delete signal, and if it is 3, it means the output is a Change signal. The corresponding data on the number of activated elements in the model below are also adjusted according to the output signal.

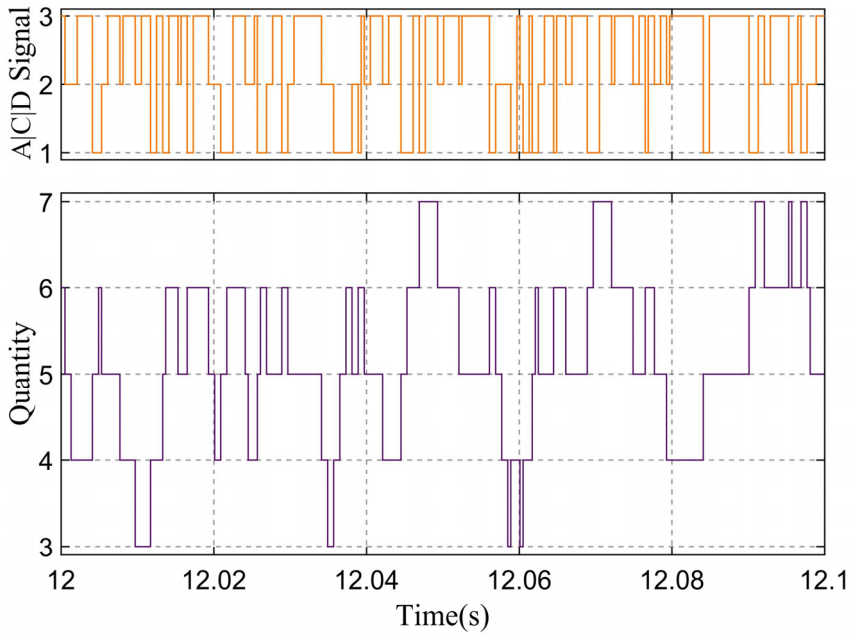

Figure 16. The output signal from quantity adaptive module and the number of active elements.

For the evaluation module and the update module, the parameters, which are worth paying attention to are the evaluation result value and the output random sequence. The model output and evaluation result values between 12 s and 12.1 s are also recorded, which are shown in Figure 17; the output of the model will be the number of injected voltage.

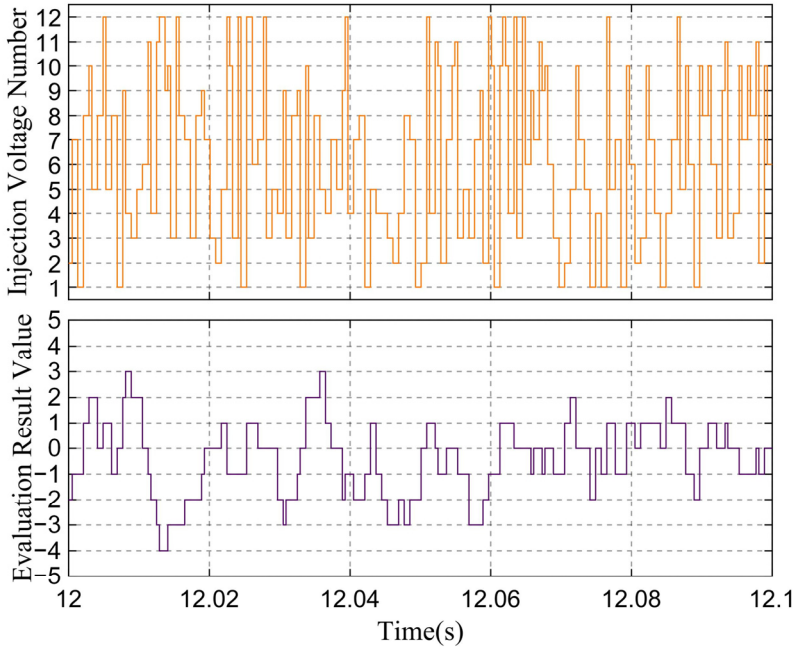

Figure 17. The evaluation result value and the injection voltage number.

From the figure, it can be seen that the evaluation value has remained stable around 0, even for an extremely long duration; there are no large or small values. The existence of such a phenomenon can ensure the rationality of the analysis of torque ripple in Section 3. The motor does not always operate under fixed operating conditions, and the parameters may also change. Maintaining an estimation result at 0 can ensure that the speed control is not subject to oscillations caused by random numbers generated by programming languages,

which can cause oscillations in the output of the speed regulator. Therefore, using this method can ignore the inductance variation in the SynRM.

6.2. Reduction in Torque Ripple and Speed Fluctuation

To illustrate, the random voltage injection sensorless control method using a self-regulating random model algorithm has a smaller amplitude on torque ripple and a smaller impact on speed control. Many comparative experiments between RVIM and SRRMM are conducted, mainly including steady state under different load conditions, start-up in stationary and reverse rotation states, and acceleration and deceleration experiments.

We used these two methods to run the motor at 100 rpm with no-load, 50% rated-load, and rated-load conditions, respectively, and record the phase current, torque, and speed. The sampling results are shown in Figure 18. In order to better display the details of each quantity, the phase current is displayed using 100 ms/div, and there is a Zoom that displays the details of the induced current caused by the injection voltages. The corresponding amplitudes for the three load conditions are 2 A/div, 3.5 A/div 5 A/div. The speed displays the duration of 5 s, while the torque displays the duration of 20 s. It can be seen that when using SRRMM, the phase current is relatively stable, while when using RVIM, there is a noticeable jitter marked by the green circle in the figure, especially when the current amplitude is large. The speed fluctuation is also relatively small when using SRRMM, only within 1.5 rpm; while using RVIM, the speed fluctuation can reach 6 rpm. The torque fluctuation is also greater for RVIM, which is about three times that of using SRRMM. It can also be seen that there is a more macroscopic fluctuation in torque when using RVIM.

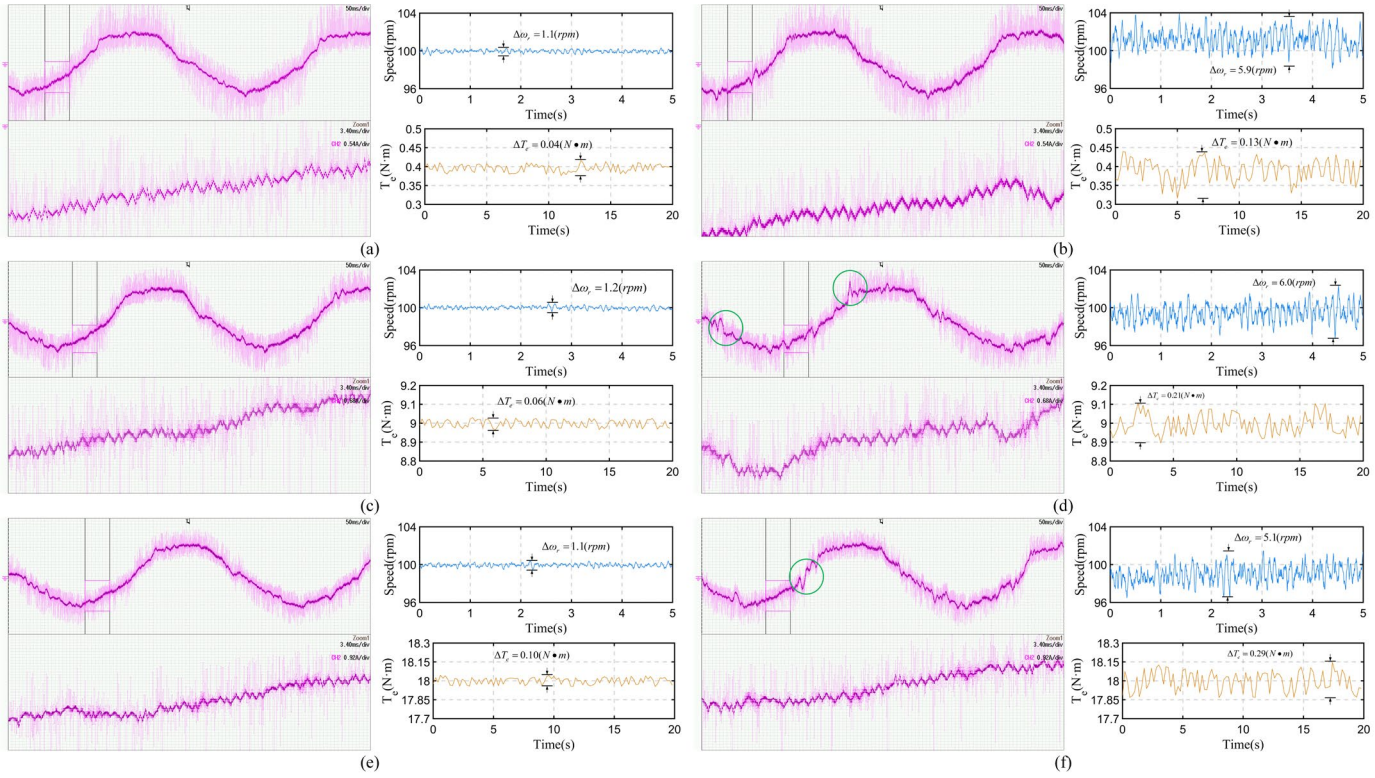

Figure 18. Sampling results of current, speed, and torque during motor running at 100 rpm. (**a**) SRRMM with no load. (**b**) RVIM with no load. (**c**) SRRMM with 50% rated load. (**d**) RVIM with 50% rated load. (**e**) SRRMM with rated load. (**f**) RVIM with rated load.

The sensorless control method proposed in this article does not require the use of methods such as I-f or V-f to start up from a stationary or negative speed state. Two control experiments are conducted, starting from a stationary state to 100 rpm and from −100 rpm to 100 rpm, respectively. The sampling images of phase current and motor speed are shown

in Figures 19 and 20. The phase current is displayed as 10 s/div in time and 2 A/div in amplitude with no load, 5 s/div in time, and 5 A/div in amplitude with rated load. The current is limited at 3.5 A with no load and 12 A with rated load. For experiments starting from the stationary state, Zoom1 displays the current at the highest speed, while Zoom2 displays the current at the steady speed. The current using SRRMM is still relatively stable, while using RVIM not only causes current jitter in a small range, but also current oscillations in a large range. Large-range current oscillations can cause significant speed oscillations, all of which are marked by green circles. Small-range current oscillations are significant with a rated load, while large-range current oscillations are significant with no load. This is because the braking force brought by the eddy current dynamometer has some filtering effect, so the speed overshoot is not significant under rated-load conditions. For experiments starting from the reverse rotation state, Zoom1 displays the current at the zero speed position, while Zoom2 displays the current at the steady speed. As before, current jitter and oscillations, as well as speed oscillations, are all marked. The speed fluctuation, which we are most concerned about, is still below 1.5 rpm when using SRRMM, while using RVIM, it even reaches 7.3 rpm in Figure 19b, and the rest is also above 5 rpm.

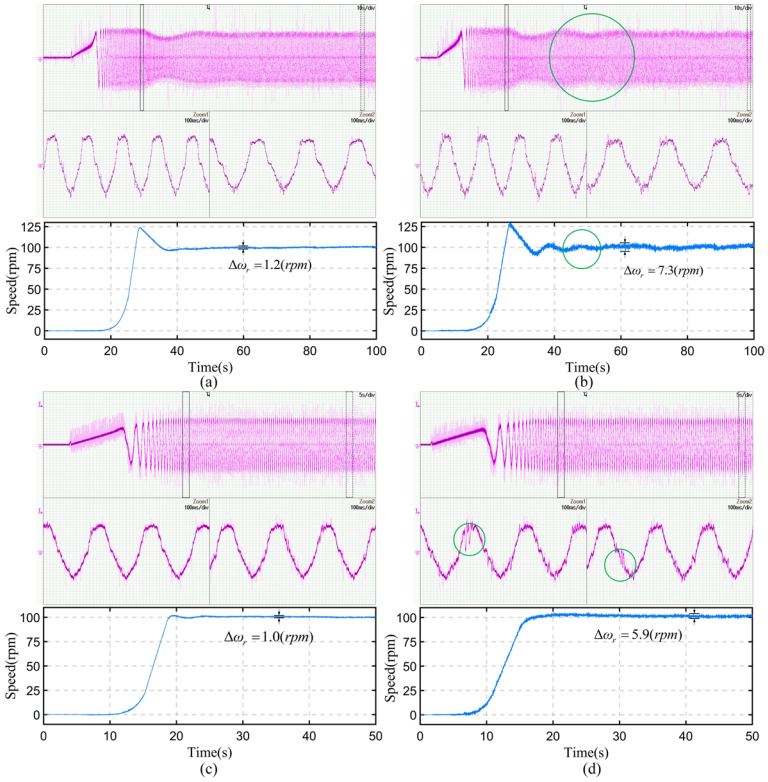

Figure 19. Sampling results of current and speed during motor start-up to 100 rpm. (**a**) SRRMM with no load. (**b**) RVIM with no load. (**c**) SRRMM with rated load. (**d**) RVIM with rated load.

Two different methods are used to conduct experiments on acceleration and deceleration between speeds of 100 rpm and 150 rpm. The experimental results are shown in Figure 21. The phase current is displayed as 10 s/div in time and 2 A/div in amplitude with no load, 5 s/div in time, and 5 A/div in amplitude with rated load. Zoom1 displays the current at 150 rpm, while Zoom2 displays the current at 100 rpm. The oscillations of speed and current are marked with green circles. For the same load situation using the same method, it can be seen that at higher speeds and currents, speed fluctuations are also greater. This confirms the analysis results of Equations (14) and (15). For using SRRMM, the speed fluctuation is about 2 rpm at the speed of 150 rpm, while for RVIM, it reaches around 7 rpm.

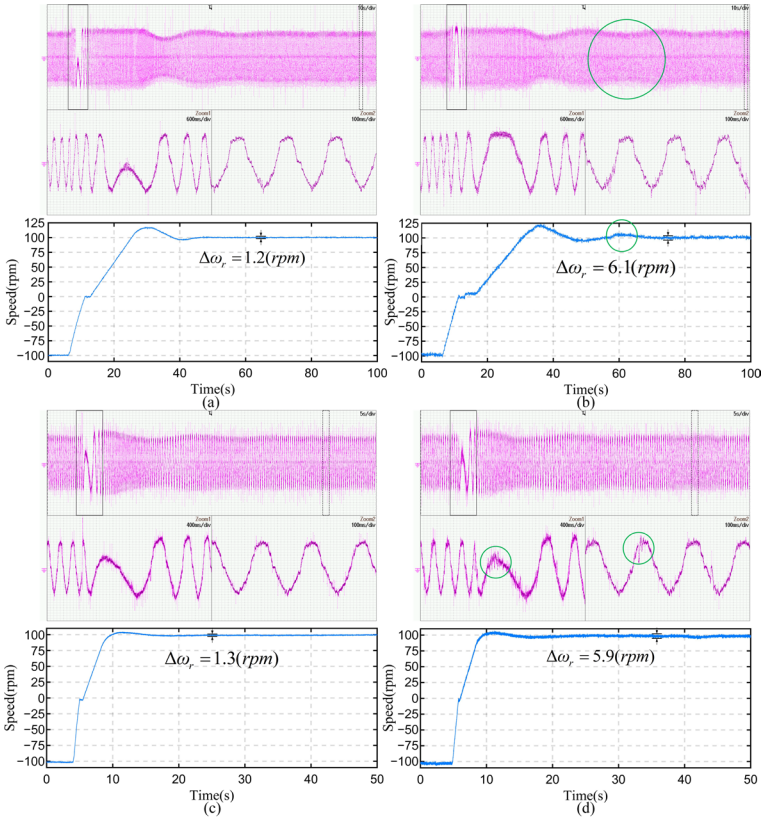

Figure 20. Sampling results of current and speed of the motor from −100 rpm to 100 rpm. (**a**) SRRMM with no load. (**b**) RVIM with no load. (**c**) SRRMM with rated load. (**d**) RVIM with rated load.

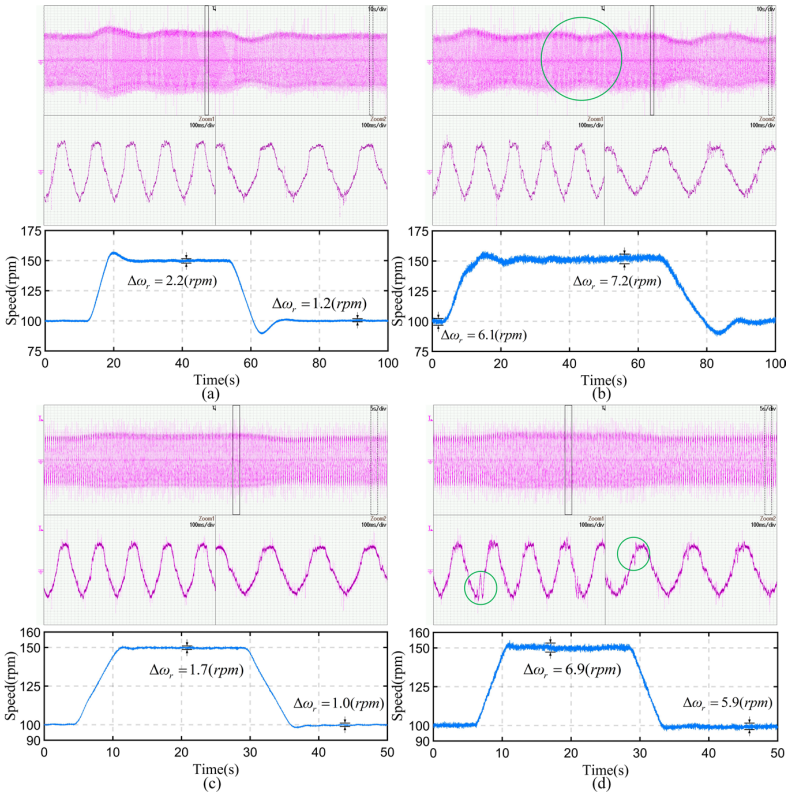

Figure 21. Sampling results of current and speed during acceleration and deceleration of the motor between 100 rpm and 150 rpm. (**a**) SRRMM with no-load. (**b**) RVIM with no-load. (**c**) SRRMM with rated load. (**d**) RVIM with rated load.

The above multiple experiments have shown that regardless of any operating state, the use of SRRMM can always maintain torque fluctuations caused by injected voltage near zero, which resists the influence of non-random or even periodic voltage selection. Therefore, the speed bias is always maintained near zero, which is beneficial for sensorless speed control.

6.3. Verification of Noise Reduction Effect Using SRRMM

In order to verify that the proposed SRRMM method can effectively suppress the noise caused by injected voltage, the following comparative experiment is designed, and all injection voltages used in the experiment are described in Table 1. The injection voltages have the frequencies of 2.5 kHz or 1.25 kHz, respectively, and to verify that the method used in this article can reduce noise, it is necessary to conduct OVIM experiments using these two different frequencies of voltages; the voltage numbers used in the two methods are 1 and 9, respectively. This method has high noise and is convenient for comparison. RVIM has been proven many times to have the function of reducing noise, and, as a commonly used method for comparison in this article, this method is conducted using all the injection voltages in Table 1. The above three methods, along with the SRRMM method proposed in this article, are all implemented under no-load and rated-load conditions. The use of two different load conditions can better demonstrate the effectiveness of the noise reduction function. When the motor runs stably at 100 rpm, acoustic noise is recorded by a sound meter Smart Sensor AS804B placed approximately 50 cm above the motor shaft; the experimental setup is shown in Figure 22, and the results are presented in Table 4. From the results, it can be seen that SRRMM, like RVIM, also has the function of reducing noise, while the noise generated by using OVIM is relatively large.

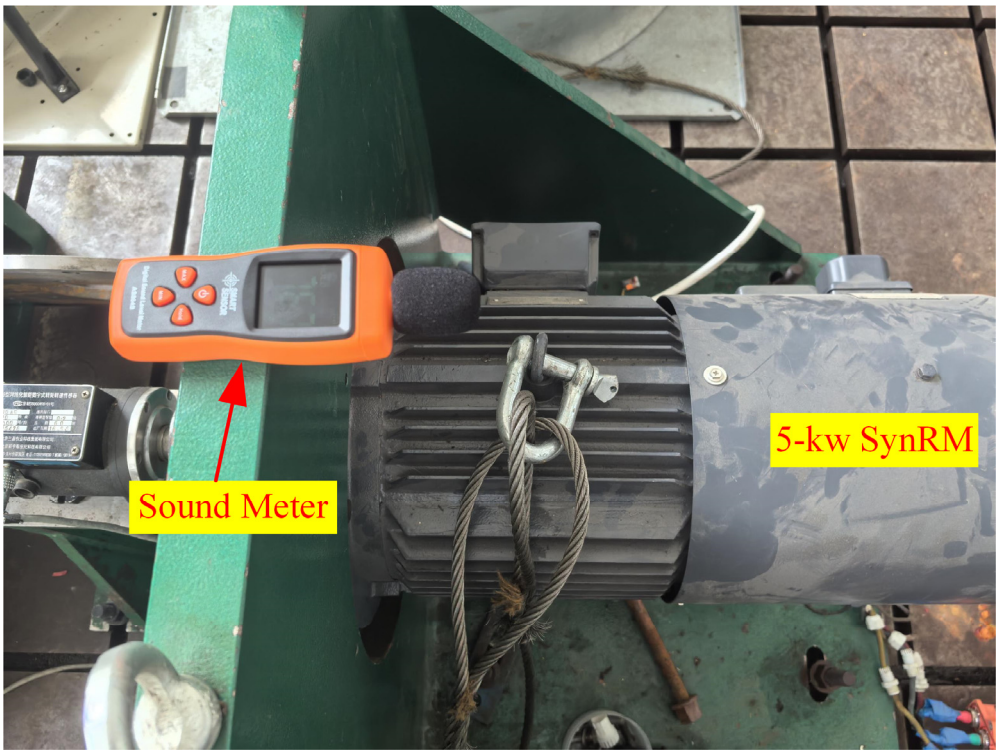

Figure 22. Collecting the noise level generated by the motor using Smart Sensor AS804B.

Table 4. The results of collecting acoustic noise levels using different methods.

Load State	No Load	Rated Load
OVIM (2.5 kHz)	76.3 dB	76.7 dB
OVIM(1.25 kHz)	76.5 dB	77.1 dB
RVIM	71.2 dB	71.4 dB
SRRMM	70.9 dB	70.9 dB

Similarly, when the motor runs stably at 100 rpm, the phase current is recorded, and the PSD and Fourier transform are calculated. As mentioned in Section 5, the calculated value of PSD is very small, and the results have been processed, they are taken the logarithm based on ten and multiplied by ten. The times of each numbered voltage are injected within 25 s and are shown in Figure 23.

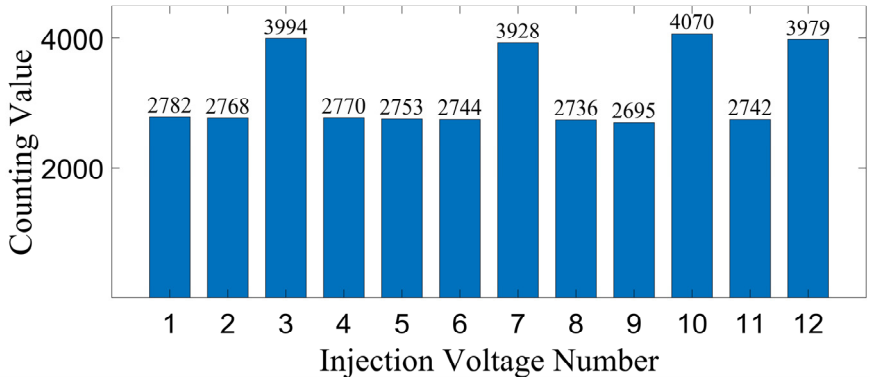

Figure 23. Record of voltage injection times for each number.

The sampled current image and the calculated PSD and Fourier transform results are shown in Figure 24. The time axis is 50 ms/div; the current axis for the no-load experiment is 2 A/div, and the rated-load experiment is 5 A/div. All current images have a Zoom to more clearly display the induced current caused by the injected voltage reflected in the phase current. The current amplitude is about 3.3 A under no-load conditions and about 9.3 A under rated-load conditions.

It can be seen from the figure that the PSD results of RVIM and SRRMM are below −60 dB in the frequency between 2 kHz and 8 kHz, which is the area where human hearing is more sensitive. From the results of the Fourier transform, it can also be seen that the current spectrum is spread out in the low-frequency range. As for the larger values at 10 kHz, they occur because the switching frequency of PWM is 10 kHz, and switching the inverter at this frequency will bring some current spikes.

The experimental results of two OVIMs show that there are significant peaks at the injection frequency and its harmonics, many of which are within the range of 2 kHz to 8 kHz. This will cause sharp noise, which is also what all random voltage methods want to eliminate.

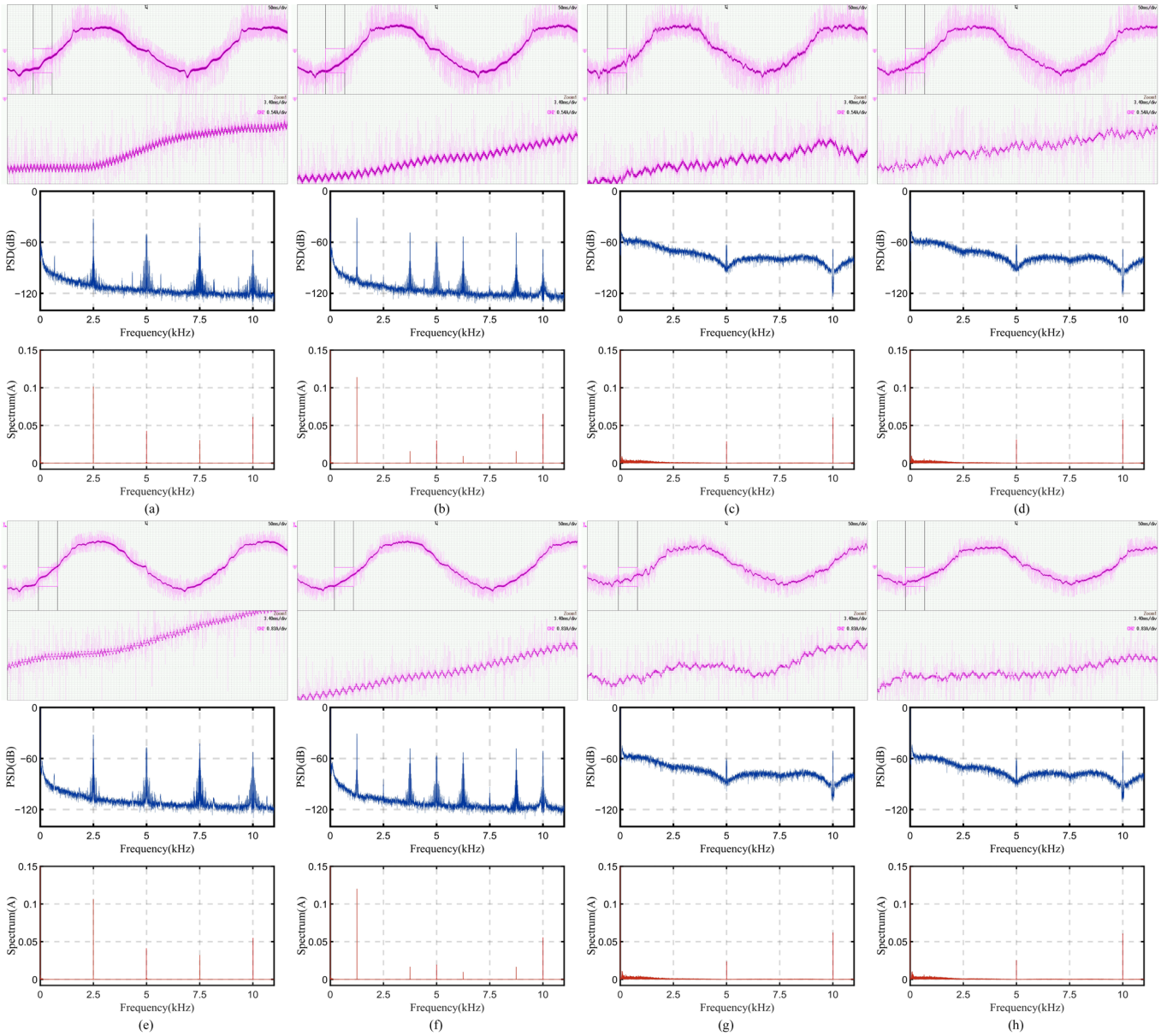

Figure 24. During steady state of the motor, phase current image, corresponding PSD calculation results, and Fourier transform results display diagram. (**a**) OVIM with 2.5 kHz injection voltage with no load. (**b**) OVIM with 1.25 kHz injection voltage with no load. (**c**) RVIM with no load. (**d**) SRRMM with no load. (**e**) OVIM with 2.5 kHz injection voltage with rated load. (**f**) OVIM with 1.25 kHz injection voltage with rated load. (**g**) RVIM with rated load. (**h**) SRRMM with rated load.

7. Conclusions

To solve the sensorless speed-control problem of synchronous reluctance motors (SynRMs) and weaken the speed bias and noise caused by injected voltage. The self-regulating random model algorithm is proposed in this paper, which can be used for sensorless control by injecting high-frequency square-wave-type voltages. This algorithm creates a model and continuously updates the activated elements within the model based on evaluation results, making the trend of the random number sequence output from the model decrease the bias of the evaluation value. Taking the torque deviation caused by induced current as the evaluation object and its impact on speed as the evaluation method, it is used to output twelve voltage numbers reasonably. This experiment has proven the feasibility of the algorithm, and the entire sensorless control method has good performance;

like other methods using random voltage, this method also has the function of reducing the noise caused by injection voltages.

Supplementary Materials: The following supporting information can be downloaded at: https://www.mdpi.com/article/10.3390/electronics13163327/s1, File S1: The Self-Regulating Random Model Algorithm proposed in this article is made into a Simulink model and compressed into zip format.

Author Contributions: Conceptualization, Y.G. (Yibo Guo); methodology, Y.G. (Yibo Guo) and L.P.; software, Y.G. (Yibo Guo) and X.C.; validation, Y.G. (Yibo Guo) and Y.Y.; formal analysis, Y.G. (Yibo Guo); investigation, Y.Y.; resources, Y.G. (Yimin Gong); data curation, Y.G. (Yibo Guo) and Y.G. (Yimin Gong); writing—original draft preparation, Y.G. (Yibo Guo); writing—review and editing, Y.G. (Yibo Guo); visualization, Y.G. (Yibo Guo) and L.P.; supervision, Y.G. (Yimin Gong); project administration, Y.Y.; funding acquisition, Y.Y. All authors have read and agreed to the published version of the manuscript.

Funding: This research received no external funding.

Data Availability Statement: The experimental data are encrypted. If there are any reasonable requests, please contact the author Yibo Guo (email: guoyb22@mails.jlu.edu.cn) for assistance. The self-regulating random model algorithm that can be used is created as a Simulink model and included in this manuscript, which can be opened through Matlab 2023a or higher versions.

Acknowledgments: Thanks to all the project team members.

Conflicts of Interest: The authors declare no conflicts of interest.

References

1. Wu, X.; Huang, S.; Liu, K.; Lu, K.; Hu, Y.; Pan, W.; Peng, X. Enhanced Position Sensorless Control Using Bilinear Recursive Least Squares Adaptive Filter for Interior Permanent Magnet Synchronous Motor. *IEEE Trans. Power Electron.* **2020**, *35*, 681–698. [CrossRef]
2. Yousefi-Talouki, A.; Boldea, I. Combined active flux and high-frequency injection methods for sensorless direct-flux vector control of synchronous reluctance machines. *IEEE Trans. Power Electron.* **2019**, *33*, 2447–2457. [CrossRef]
3. Ichikawa, S.; Okuma, S. Sensorless control of synchronous reluctance motors based on extended EMF models considering magnetic saturation with online parameter identification. *IEEE Trans. Ind. Appl.* **2006**, *42*, 1264–1274. [CrossRef]
4. Wang, D.; Lu, K.; Rasmussen, P.O. Improved Closed-Loop Flux Observer Based Sensorless Control Against System Oscillation for Synchronous Reluctance Machine Drives. *IEEE Trans. Power Electron.* **2019**, *34*, 4593–4602.
5. Varatharajan, A.; Pellegrino, G.; Armando, E. Sensorless synchronous reluctance motor drives: Auxiliary flux-based position observer. *IEEE J. Emerg. Sel. Top. Power Electron.* **2021**, *9*, 4330–4339. [CrossRef]
6. Zhang, Z.; Lamb, J. Active Q Flux Concept for Sensorless Control of Synchronous Reluctance Machines. *IEEE Trans. Ind. Electron.* **2023**, *70*, 4526–4536. [CrossRef]
7. Gao, F.; Yin, Z.; Bai, C.; Yuan, D.; Liu, J. A Lag Compensation-Enhanced Adaptive Quasi-Fading Kalman Filter for Sensorless Control of Synchronous Reluctance Motor. *IEEE Trans. Power Electron.* **2022**, *37*, 15322–15337. [CrossRef]
8. Pasqualotto, D.; Rigon, S.; Zigliotto, M. Sensorless Speed Control of Synchronous Reluctance Motor Drives Based on Extended Kalman Filter and Neural Magnetic Model. *IEEE Trans. Ind. Electron.* **2023**, *70*, 1321–1330. [CrossRef]
9. Foti, S.; De Caro, S.; Scimone, T.; Testa, A.; Tornello, L.D.; Scelba, G.; Cacciato, M. Rotor Position Error Compensation in Sensorless Synchronous Reluctance Motor Drives. *IEEE Trans. Power Electron.* **2022**, *37*, 4442–4452. [CrossRef]
10. Yousefi-Talouki, A.; Pescetto, P.; Pellegrino, G. Sensorless Direct Flux Vector Control of Synchronous Reluctance Motors Including Standstill, MTPA, and Flux Weakening. *IEEE Trans. Ind. Appl.* **2017**, *53*, 3598–3608. [CrossRef]
11. Chen, J.; Fan, Y.; Wang, W.; Lee, C.H.T.; Wang, Y. Sensorless Control for SynRM Drives Using a Pseudo-Random High-Frequency Triangular-Wave Current Signal Injection Scheme. *IEEE Trans. Power Electron.* **2022**, *37*, 7122–7131. [CrossRef]
12. Yoon, Y.-D.; Sul, S.-K.; Morimoto, S.; Ide, K. High-Bandwidth Sensorless Algorithm for AC Machines Based on Square-Wave-Type Voltage Injection. *IEEE Trans. Ind. Appl.* **2011**, *47*, 1361–1370. [CrossRef]
13. Li, C.; Wang, G.; Zhang, G.; Zhao, N.; Xu, D. Adaptive Pseudorandom High-Frequency Square-Wave Voltage Injection Based Sensorless Control for SynRM Drives. *IEEE Trans. Power Electron.* **2021**, *36*, 3200–3210. [CrossRef]
14. Zhang, G.; Xiang, R.; Wang, G.; Li, C.; Bi, G.; Zhao, N.; Xu, D. Hybrid Pseudorandom Signal Injection for Position Sensorless SynRM Drives With Acoustic Noise Reduction. IEEE Trans. Transport. *Electrification* **2022**, *8*, 1313–1325.
15. Zhang, Y.; Yin, Z.; Liu, J.; Zhang, R.; Sun, X. IPMSM Sensorless Control Using High-Frequency Voltage Injection Method With Random Switching Frequency for Audible Noise Improvement. *IEEE Trans. Ind. Electron.* **2020**, *67*, 6019–6030. [CrossRef]
16. Lv, L.; Hu, Z.; Li, S.; Guo, R.; Wang, J.; Wang, G.; Li, S. Variable-Angle Random High-Frequency Voltage Injection Strategy with Cross-Saturation Effect Compensation for Sensorless Synchronous Reluctance Motor Drives. *Energies* **2024**, *17*, 725. [CrossRef]

17. Li, C.; Wang, G.; Zhang, G.; Xu, D.; Xiao, D. Saliency-Based Sensorless Control for SynRM Drives With Suppression of Position Estimation Error. *IEEE Trans. Ind. Electron.* **2019**, *66*, 5839–5849. [CrossRef]
18. Li, C.; Wang, G.; Zhang, G.; Zhao, N.; Gao, Y.; Xu, D. Torque Ripples Minimization of Sensorless SynRM Drives for Low-Speed Operation Using Bi-HFSI Scheme. *IEEE Trans. Ind. Electron.* **2021**, *68*, 5559–5570. [CrossRef]
19. Varatharajan, A.; Pellegrino, G.; Mariani, G.B.; Voyer, N.; Satake, A. LUT-Less Sensorless Control of Synchronous Reluctance Machines Using the Locus of Incremental Saliency Ratio Tracking (LIST). *IEEE Trans. Ind. Electron.* **2022**, *69*, 6530–6539. [CrossRef]
20. Bugsch, M.; Piepenbreier, B. High-Bandwidth Sensorless Control of Synchronous Reluctance Machines in the Low- and Zero-Speed Range. *IEEE Trans. Ind. Appl.* **2020**, *56*, 2663–2672. [CrossRef]
21. Lin, Z.; Li, X.; Wang, Z.; Shi, T.; Xia, C. Minimization of Additional High-Frequency Torque Ripple for Square-Wave Voltage Injection IPMSM Sensorless Drives. *IEEE Trans. Power Electron.* **2020**, *35*, 13345–13355. [CrossRef]
22. Chen, Q.; Yan, Y.; Xu, G.; Xu, M.; Liu, G. Principle of Torque Ripple Reduction in Synchronous Reluctance Motors With Shifted Asymmetrical Poles. *IEEE J. Emerg. Sel. Top. Power Electron.* **2020**, *8*, 2611–2622. [CrossRef]
23. Qu, J.; Zhang, C.; Jatskevich, J.; Zhang, S. Deadbeat Harmonic Current Control of Permanent Magnet Synchronous Machine Drives for Torque Ripple Reduction. *IEEE J. Emerg. Sel. Top. Power Electron.* **2022**, *10*, 3357–3370. [CrossRef]
24. Woo, T.-G.; Park, S.-W.; Choi, S.-C.; Lee, H.-J.; Yoon, Y.-D. Flux Saturation Model Including Cross Saturation for Synchronous Reluctance Machines and Its Identification Method at Standstill. *IEEE Trans. Ind. Electron.* **2023**, *70*, 2318–2328. [CrossRef]
25. Hinkkanen, M.; Pescetto, P.; Mölsä, E.; Saarakkala, S.E.; Pellegrino, G.; Bojoi, R. Sensorless Self-Commissioning of Synchronous Reluctance Motors at Standstill Without Rotor Locking. *IEEE Trans. Ind. Appl.* **2017**, *53*, 2120–2129. [CrossRef]
26. Hwang, C.-E.; Lee, Y.; Sul, S.-K. Analysis on Position Estimation Error in Position-Sensorless Operation of IPMSM Using Pulsating Square Wave Signal Injection. *IEEE Trans. Ind. Appl.* **2019**, *55*, 458–470. [CrossRef]
27. Tse, K.K.; Chung, H.S.-H.; Huo, S.Y.; So, H.C. Analysis and spectral characteristics of a spread-spectrum technique for conducted EMI suppression. *IEEE Trans. Power Electron.* **2000**, *15*, 399–410. [CrossRef]
28. Tse, K.K.; Chung, H.S.-H.; Hui, S.Y.R.; So, H.C. A comparative investigation on the use of random modulation schemes for DC/DC converters. *IEEE Trans. Ind. Electron.* **2000**, *47*, 253–263. [CrossRef]

Disclaimer/Publisher's Note: The statements, opinions and data contained in all publications are solely those of the individual author(s) and contributor(s) and not of MDPI and/or the editor(s). MDPI and/or the editor(s) disclaim responsibility for any injury to people or property resulting from any ideas, methods, instructions or products referred to in the content.